Probable rotation states of rocket bodies in Low Earth Orbit

Dr. Gregory W Ojakangas[1*], Dr. P. Anz-Meador[2], Dr. H. Cowardin[2]
[1] Drury University/LZ Technology,[2]ESCG/Jacobs   *email: gojakang@drury.edu

Abstract:

In order for Active Debris Removal to be accomplished, it is critically important to understand the probable rotation states of orbiting, spent rocket bodies (RBs). However, rotational dynamics is non-intuitive and misconceptions are common. Determinations of rotation and precession rates have been published that are physically impossible. In a state of free precession, the total angular momentum of the object is constant, while kinetic energy decreases due to internal friction, approaching rotation about the axis of maximum inertia. For solid internal friction the timescale is hundreds to thousands of years for quality factors of ~100 and assuming metallic rigidities, but for turbulent friction in partially-filled liquid fuel tanks we predict that the preferred rotational state is approached rapidly, within days to months. However, history has shown that theoretical predictions of the timescale have been notoriously inaccurate. In free precession, the 3-1-3 Euler angle rates $\dot{\varphi}$ (precession rate of long axis about fixed angular momentum with cone angle θ) and $\dot{\psi}$ (roll rate around long axis) have comparable magnitudes until very close to θ=π/2, so that otherwise the true "rotation period" is not simply twice the primary light curve period. Furthermore $\dot{\theta}$, nonzero due to friction, becomes asymptotically smaller as θ=π/2 is approached, so that θ can linger within several degrees of flat spin for a relatively long time. Such a condition is likely common, and cannot be distinguished from the "wobble" of a cylinder with a skewed inertia tensor unless the RB has non-axisymmetric reflectivity characteristics. For an RB of known dimensions, a given value of θ fixes the relative values of $\dot{\varphi}$ and $\dot{\psi}$. In forced precession, the angular momentum precesses about a symmetry axis defined by the relevant torque. However, in LEO, only gravity gradient and magnetic induction torques are dominant, and these cannot cause precession periods shorter than a week, or more likely, months. Thus forced precession is probably not observable over observation campaigns spanning a few days or less. Building on Smith [7] an expression for the magnetic induction torque on an arbitrarily rotating cylinder, hitherto not available in the literature, is presented here. Numerical integrations of the equations of motion for a cylindrical RB in LEO with arbitrary initial conditions and subject to magnetic and gravity gradient torques as well as prescribed internal dissipation are in progress. Acknowledgements: This work was produced under NASA contract NNJ05HI05.

1. Introduction

The task of Active Debris Removal [1] will be greatly aided by a detailed knowledge of the rotational states of rocket bodies (RBs) which are designated for removal from orbit. For this reason, there has been much recent work in the space surveillance community on the problem of determining RB rotation states from light curves (e.g. [2]-[4]). However, these rotation states are at present inadequately understood. We focus here on the abundant Soviet SL-8's. The primary phenomena influencing the rotational evolution of RB's in LEO are the torques due to magnetically-induced eddy currents and the gravitational gradient, as well as the effects of internal friction within the body.   In LEO, torque due to solar radiation pressure is probably at least two orders of magnitude or more smaller than the smallest of these effects.

Much groundbreaking work on the rotational evolution of RBs was performed five decades ago, at the start of the U.S. space program. For example, analytical predictions were performed [5,6,7] of rotational evolution of spherical and cylindrical RBs under the influence of the eddy current torques resulting from motion of the satellite through the earth's magnetic field. While these analytical calculations are elegant, they are limited to rotation states in which the angular velocity remains constant over an orbit period, so magnetic field components can be averaged over that period. Furthermore, the torques were only calculated in [7] for the states of spin-stabilization about the long axis, and for pure end-over-end (flat spin) tumble. Because of these limiting assumptions, the full spin evolution of an arbitrarily-rotating cylindrical RB cannot be investigated with these results, and they certainly cannot apply to bodies precessing significantly within an orbit period.

Torques due to atmospheric drag forces are only comparable to eddy current torques at altitudes below about 160km [8], so they are ignorable in this work. The dynamics of satellite orientation under the influence of gravity gradient

torque is of paramount importance in satellite control, so this influence was investigated in detail many decades ago as well (cf. [9]). However, its relevance to interpretation of light curves from RBs in LEO bears investigation, since its magnitude can be as large as that of magnetic induction, and that spin-orbit resonances may be a factor in light curve interpretation.

2. "Much confusion about precession" , or "Free and forced precession"

To understand the rotation states of RBs and their corresponding light curves, it is valuable to examine the essential similarities and differences between free precession and forced precession, as well as realistic rates that each might exhibit. Since RBs typically have nearly cylindrical symmetry, their rotational dynamics are well approximated by those of a symmetric top, and are treated as such here. In a state of *free precession* the angular momentum L of the body remains constant in inertial space, while the angular velocity ω and body symmetry axis x_{3b} precess about L at a rate commonly referred to as the free precession rate:
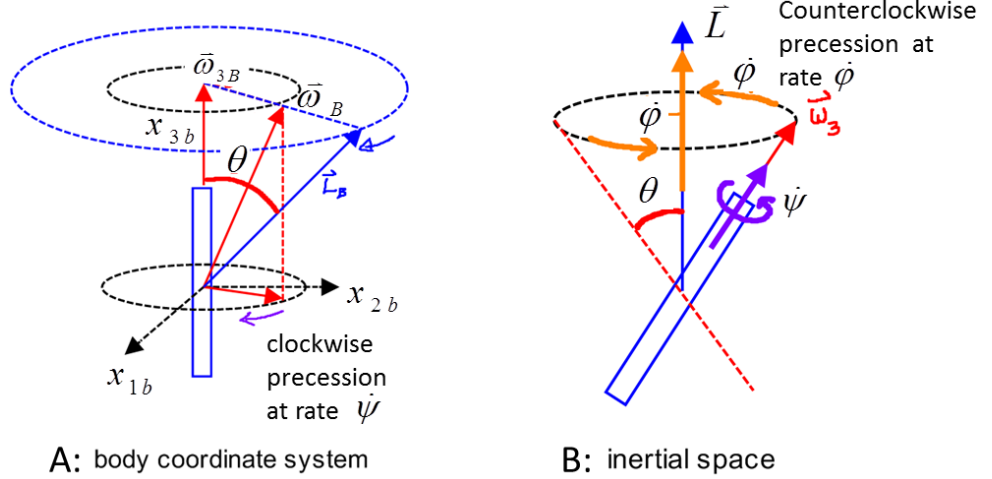
Fig.1: Free precession viewed in the body coordinate system (A) and in inertial space (B). The view in (B) is directly relevant to telescopic observations, while (A) is not.

$$\omega_0 = \frac{\Delta I}{I_0}\omega_{3b} \tag{1}$$

where I_o is the maximum rotational inertia and ΔI is the difference between the maximum and axial inertia components : $\Delta I = I_0 - I_3$. Thus for positive ΔI, the precession of ω and L about x_{3b} is clockwise as seen in Fig.1a. Because of the ease with which this result is obtained from the Euler equations, this is commonly the extent of the treatment of free precession in introductory dynamics textbooks (cf. [10]), but it is not useful for observations of the phenomenon from inertial space as in telescopic observations. However, if we define a 3-1-3 Euler angle sequence using the standard angles φ, θ and ψ (where the inertial z-axis is parallel to L), then by equating the components of ω in the body coordinate system, found in the above-mentioned development, to the the *vector* $\vec{\varphi} + \vec{\psi}$, also expressed in the body coordinate system, the following results are readily obtained:

$$\dot{\varphi} = L\!\!\Big/\!\!I_0 \tag{2}$$

$$\dot{\psi} = \omega_0 = \frac{\Delta I}{I_0}\omega_{3b} = \frac{\Delta I}{I_3}\dot{\varphi}\cos\theta \tag{3}$$

where

$$\cos\theta = \frac{I_3\omega_{3b}}{L} \tag{4}$$

The roll-rate about the symmetry axis, $\dot{\psi}$, is thus seen to be identical to the free precession rate ω_0, so if $\dot{\psi}$ is positive in inertial space (counterclockwise axial roll as seen from above x_{3b}), then, for the usual case: $0 < \theta < \pi/2$, the x_{3b} axis also precesses in the positive (counterclockwise) sense about L in the inertial coordinate system, at the rate $\dot{\varphi}$ as seen in Fig.1b. Both $\dot{\varphi}$ and $\dot{\psi}$ can be referred to as "precession rates", leading to the need for

researchers to explain which meaning they are employing when they refer to free precession. For SL-8s, $\Delta I / I_3 \sim 4.3$, and Eqs (2) and (3) indicate that $\dot{\psi}$ can be a larger component of the angular velocity than $\dot{\varphi}$, unless θ is very close to $\pi/2$. The above equations can be cast in an even more useful form by using the expressions for kinetic energy E and the square of L in the body coordinate system:

$$E = \frac{1}{2} I_0 \left(\omega_{1b}^2 + \omega_{2b}^2 \right) + \frac{1}{2} I_3 \omega_{3b}^2 \qquad (5)$$

and

$$L^2 = I_0^2 \left(\omega_{1b}^2 + \omega_{2b}^2 \right) + I_3^2 \omega_{3b}^2 \qquad (6)$$
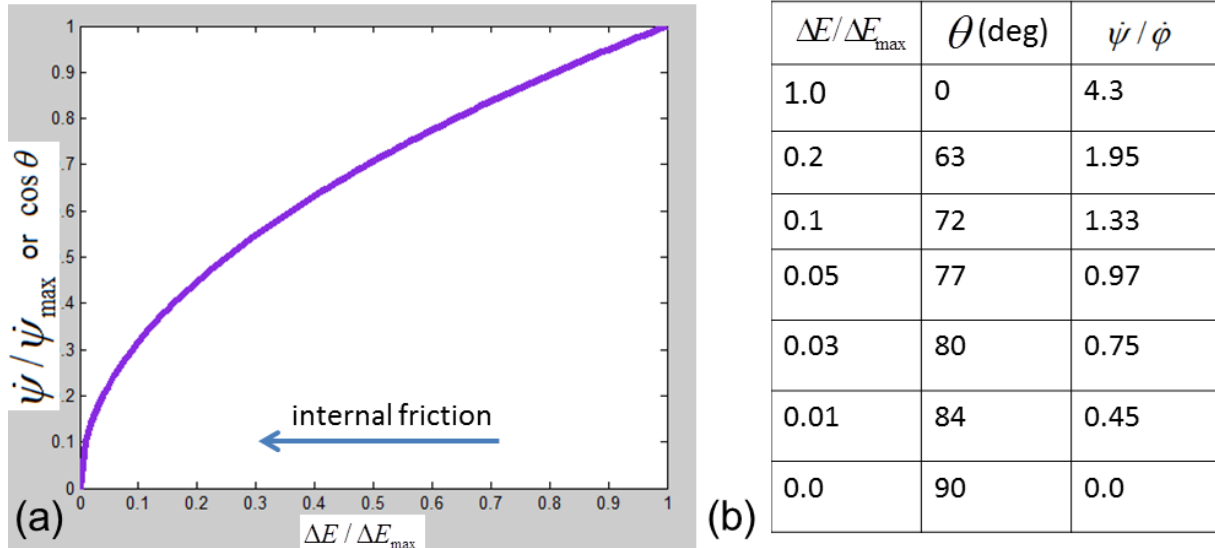
We also define the difference between the actual kinetic energy and its minimum possible value as ΔE:

$$\Delta E \equiv E - \frac{L^2}{2 I_0} \qquad (7)$$

Combining Eqs. (5) - (7) with (2) – (4) yields

$$\dot{\psi} = \sqrt{\frac{2 \Delta I \Delta E}{I_0 I_3}} \qquad (8)$$

and

$$\cos \theta = \frac{1}{L} \sqrt{\frac{2 \Delta E I_0 I_3}{\Delta I}} \qquad (9)$$

| $\Delta E / \Delta E_{max}$	θ (deg)	$\dot{\psi} / \dot{\varphi}$
1.0	0	4.3
0.2	63	1.95
0.1	72	1.33
0.05	77	0.97
0.03	80	0.75
0.01	84	0.45
0.0	90	0.0

Figure 2a: dependence of $\dot{\psi}$ and $\cos\theta$ on ΔE. Both quantities maintain substantial magnitudes until very close to minimum energy. Note in (b) that even with only 1% of maximum ΔE remaining, θ is still 16 degrees from a flat spin, and the roll-rate $\dot{\psi}$ is 45% of $\dot{\varphi}$.

Eqs (2), (8) and (9) provide considerable insight into the nature of free precession as the energy is reduced by internal friction toward its minimum value at $\Delta E = 0$. Fig.2a shows the square-root dependence of $\dot{\psi}$ and $\cos\theta$ on the kinetic energy. Consequently, both quantities remain relatively large until ΔE is very close to zero. Furthermore,

it is shown below that the rate of internal dissipation is also a decreasing function of θ, so that loss of kinetic energy is probably much slower as θ approaches π/2, contributing further to the persistence of a relatively large roll-rate.

A rather remarkable fact revealed by these equations is that $\dot\varphi$ remains constant as energy is reduced. Note that since $\dot\varphi$ is the rate of end-over-end rotation when θ is close to π/2, in that common situation it is the angular rate that most strongly modulates an RB light curve, so it is frequently identified as twice the "rotation rate". However, since $\dot\psi$ is of comparable magnitude to $\dot\varphi$ until very close to θ=π/2, it is incorrect to identify $\dot\varphi$ with the rotation rate. In fact, the true rotation rate can be written

$$\omega = \sqrt{\dot\varphi^2 + \dot\psi^2 + 2\dot\varphi\dot\psi\cos\theta} = \dot\varphi\sqrt{1 + \frac{\Delta E}{\Delta E_{max}}\frac{I_0 + I_3}{I_3}} \qquad (10)$$
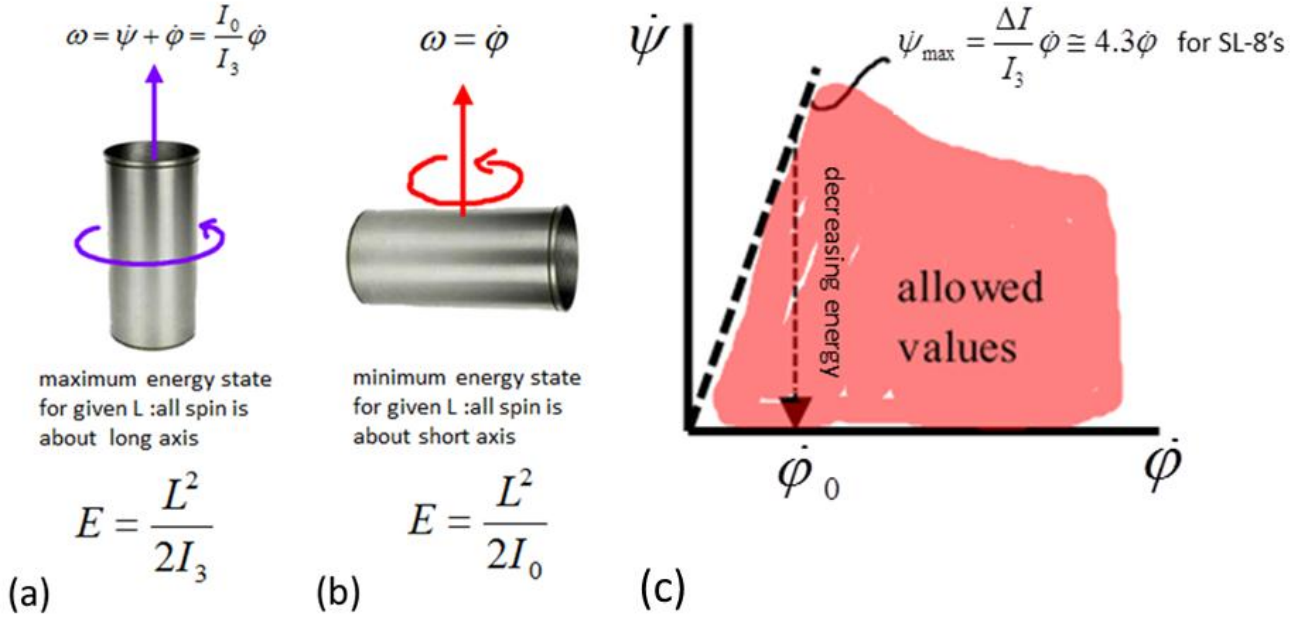
Figure 4:(a) maximum energy state corresponds to axial spin stabilization. (b) minimum energy state is pure end-over-end tumble. (c) evolution of $\dot\psi$ versus $\dot\varphi$.

Fig.3a shows the case of maximum rotational energy ($\Delta E=\Delta E_{max}$, θ=0) which corresponds to spin stabilization about the axis of symmetry, and Fig.3b shows the case of minimum rotational energy ($\Delta E=0$, θ=π/2) which corresponds to pure end-over-end tumble. Note that in the limiting case (a) when θ =0, $\dot\psi$ and $\dot\varphi$ both represent rotation about the symmetry axis, and $\dot\psi = (\Delta I/I_3) \dot\varphi$. Fig.3c shows the allowed values of $\dot\psi$ and $\dot\varphi$.

In free precession, **L** must remain along the inertial z axis. Therefore, horizontal components of angular momenta about long and short axes must cancel. This is why $\dot\psi$ and $\dot\varphi$ have similar values until pure tumble is approached. It is easy to show that this requirement leads to recovery of Eq. (3). The practical consequence is that claims of large light-curve-derived values of "rotation rate", with θ *not* near π/2 together with relatively small "precession rate" (e.g. [4]) are impossible in a state of free precession. In fact the value of $\dot\psi$ is fixed once $\dot\varphi$ and θ are determined.

3.Internal friction
The time evolution of the rotation state can be understood through Eqs. (8) and (9) if the rate of internal friction is known. While it is difficult to ascribe a precise mathematical expression to the dissipation, the amount and mathematical form of dissipation due to various phenomena can be roughly estimated.

Energy loss due to solid internal friction can be estimated as follows: The time-varying stress within a freely precessing cylindrical shell of radius R and length H is due to the difference in centripetal acceleration between mass elements close to the angular momentum axis and those far from it, experienced across the diameter of the RB. This difference scales as

$$\Delta a_c \approx \dot{\varphi}^2 2R\cos\theta \tag{11}$$

This leads to a difference in centrifugal force felt by one side of the RB relative to the other of roughly half the mass m of the RB times Δa_c, and this differential force is applied across a characteristic area A ~ Hd (cylinder is hollow), where H and d are the length and thickness of the cylindrical shell. Dividing (m/2) Δa_c by A gives the characteristic time-varying stress σ, which varies roughly sinusoidally with the free-precession rate:

$$\sigma = \sigma_0 \cos\omega_0 t \tag{12}$$

where

$$\sigma_0 \approx 2\pi R^2 \rho \dot{\varphi}^2 \cos\theta \tag{13}$$

and ρ is the material density of the cylinder. The accompanying strain scales as

$$\varepsilon \approx \frac{\sigma_0}{\mu}\cos\left(\omega_0 t - \frac{1}{Q}\right) \tag{14}$$

Where μ is the rigidity of the shell and 1/Q is the phase lag between stress and strain. Q is the quality factor for the material of which the shell is constructed. The average value of the stress times the strain rate, integrated over one precession period, yields an estimate of the volumetric dissipation rate within the RB due to solid friction. Multiplying this rate by the characteristic volume of the RB shell, V_{rb} ~2πRHd gives the estimate of total dissipation rate due to solid friction. This is related to the rate of change of θ by the chain rule:
Using Eqs. 2 and 3, the result can then be written

$$\frac{d\theta}{dt} = \frac{d\theta}{dE}\frac{dE}{dt} \approx \frac{1}{\tau_e}\frac{\cos^2\theta}{\sin\theta} \tag{15}$$

where

$$\tau_e = \frac{\mu Q H d I_0^4}{2\pi m^2 R^3 L^3} \tag{16}$$

τ_e is ~ 10^2 - 10^3 years for typical parameters relevant to SL-8s and using Q~100 and the rigidity of Aluminum. Eq.(15) is easily integrated, giving:

$$\theta = \cos^{-1}\left(\frac{1}{1+\dfrac{t}{\tau_e}}\right) \tag{17}$$

The result is plotted in Fig.4a.

A more significant source of friction is likely generated by the motion of residual fuel and oxidizer in on-board propellant tanks. This is an effect that is of great importance in the aerospace industry, yet analytic attempts to quantify its magnitude have met with modest success only when combined with laboratory experiments [11]. It is helpful, however, to examine its functional form with scaling arguments. We initially consider the liquid to reside within the end(s) of the hollow cylindrical shell, filling the cylinder to a fractional height *f*. Motion is initially assumed to be confined to an Ekman boundary layer of thickness

$$\delta = \sqrt{\frac{2\pi}{\dot{\varphi}}\nu} \tag{18}$$

where ν is the kinematic viscosity of the fluid. For dimethyl hydrazine $\nu = 6\times10^{-6} m^2/sec$ (Wikipedia reference). In the above expression the rotation rate is approximated by $\dot{\varphi}$. The characteristic amplitude of the fluid velocity relative to the interior surface is

$$V_{rel} \approx (2R)/(2\pi/\dot{\psi})$$ (19)

The viscous stress in the boundary layer is then approximately

$$\sigma \approx \eta V_{rel}/\varsigma$$ (20)

and the strain rate is simply the stress divided by the dynamic viscosity. Summing the product over the volume of the boundary layer $2\pi RH\delta$ gives an estimate of the total dissipation rate. Again using the chain rule, we obtain

$$\frac{d\theta}{dt} = \frac{d\theta}{dE}\frac{dE}{dt} \approx \frac{1}{\tau_v}\frac{\cos\theta}{\sin\theta}$$ (21)

where

$$\tau_v = \frac{(\pi I_0)^{3/2} I_3}{\sqrt{2}\rho_f R^3 Hf\Delta I(\nu L)^{1/2}}$$ (22)

where ρ_f is the density of the fuel or oxidizer and the fluid motion can be shown to be nonturbulent (Reynolds number ~40). τ_v is a few hours for f~0.1 and using the density and viscosity of dimethyl hydrazine. It has indeed been found that transition to flat spin can happen very quickly (within 5 minutes) in an initially spin-stabilized RB loaded with a large volume of fuel [11]. However, for the case of SL-8s, the fuel is in auxiliary tanks that are a fraction of ~1/8 of the cylinder radius. Since τ_v scales as the inverse cube of the radius, we may estimate that the timescale is ~8^3 times longer than that given by equation x, thus increasing the timescale to perhaps a few months.

Eq.(21) is readily integrated analytically, giving

$$\theta = \cos^{-1}[\exp(-t/\tau_v)]$$ (23)

Figs.4a,b illustrate the behavior of the coning angle θ as functions of scaled time for solid and viscous internal friction. While these functional forms should not be assumed to be highly accurate, they serve to illustrate how θ may linger for an extended time within several degrees of π/2. Consequently, from Eq.(3), a significant axial roll rate $\dot{\psi}$ will also persist.
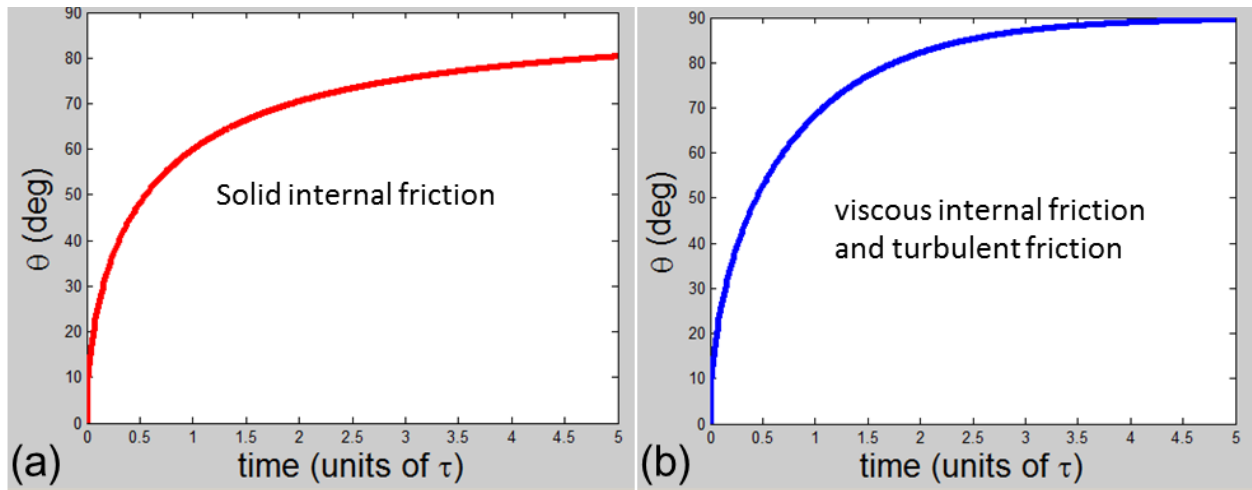
4. Free precession versus offset inertia matrix

Fig. 6: Evolution of θ with solid internal friction (a) and fluid internal friction (b). Note that θ may linger close to 90 degrees for an extended period in both cases.

It has become evident from observations that a significant number of RBs are not in a rotation state of pure end-over-end tumble. The results described above suggest that this may be due to values of θ that remain significantly different from π/2 for extended periods of time. Another possibility that has been recently considered [12] is that RBs may have principal axes of inertia that are offset from the symmetry axes by a small angle, due to asymmetric mass distributions within the body. An interesting question is whether such motion, defined here as "wobble", is distinguishable from free precession. We simulate wobbling bodies that are in a state of minimum energy rotation with a prescribed angular velocity direction as shown in Fig.5. We define the "home" position of an RB such that the (x_{1b}, x_{2b}, x_{3b})- body axes are coincident with those of a chosen inertial coordinate system (see Section 8). We then reorient the body through the series of four rotations shown in the figure. The first three rotations bring the RB to a state where the y_b-axis is directed according to the chosen angular velocity. The fourth rotation, represented by δ in the figure, is spin about the chosen axis. A fifth rotation tips the object by the "wobble angle" referred to as α_w
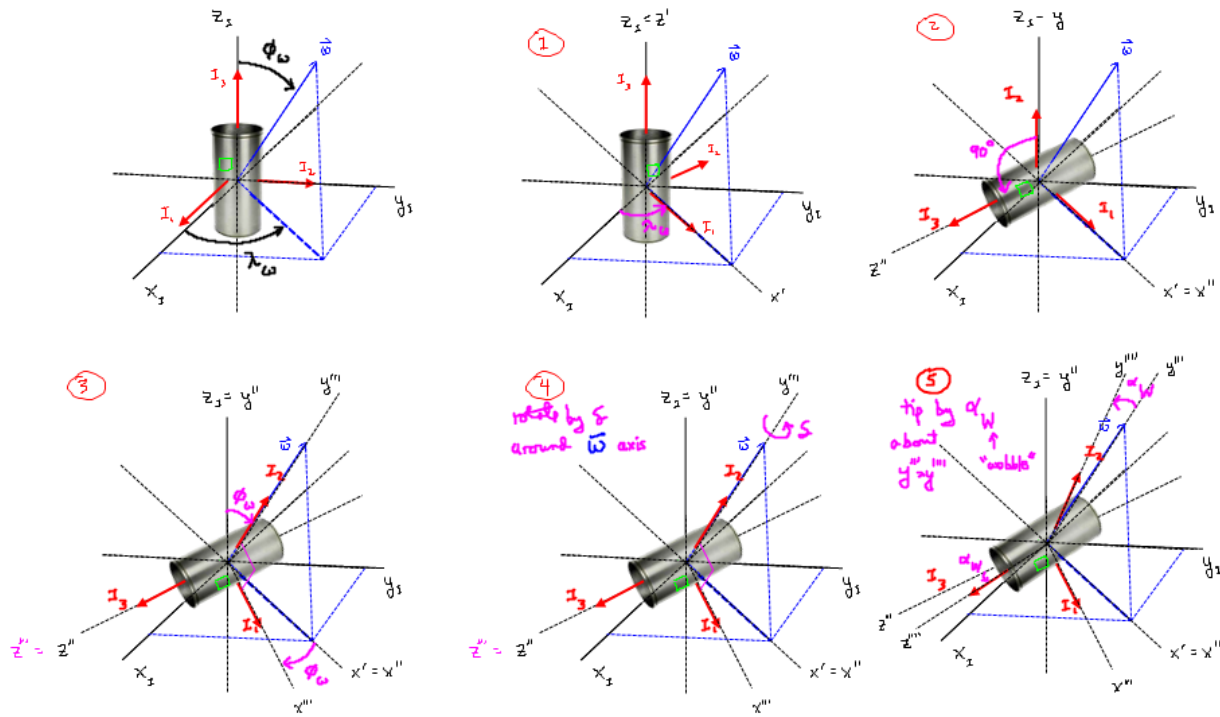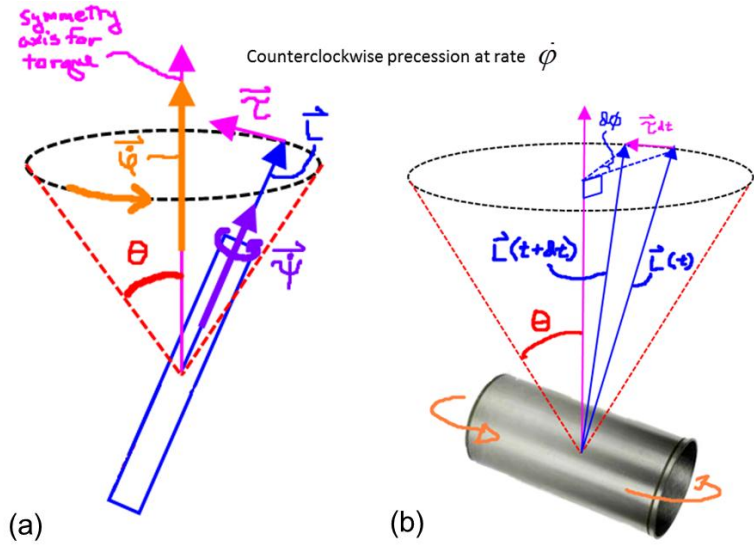

Fig. 7: Series of rotations used to place an RB in a state of "wobble" – i.e., rotating stabley about the maximum axis of inertia, where that axis is offset from a symmetry axis. The direction of the angular velocity is specified in inertial space by polar angles λ_ω and φ_ω.

These rotations are employed in section 9 to simulate light curves from wobbling versus non-wobbling RBs. Examination of Eqs (1)–(3) quickly reveals that the only observational difference between the light curve of a freely precessing cylinder with coning angle θ, and a "wobbling" cylinder with a wobble angle of π/2-θ, will be if the cylinder has a non-axisymmetric reflectivity pattern. Further research will investigate whether the larger cross-sectional area when saddle tanks of an SL-8 are visible, leads to enough of a modulation of the signal intensity to be readily identified. Initial estimates indicate an approximately ~25% increase in reflected intensity due to that effect. A useful fact is that if $\dot\varphi$ and θ are determined from the light curve data, the signature of the axial roll should have the prescribed frequency given by Eq.(3). This signature could of course be sought in FFT data of light curves. Another possible signature that would identify a non-zero roll rate would be the insignias on one side of the RB. For protection, such insignias are emplaced on the side opposite the launch tower [13] but it is not known how long they persist under the harsh conditions of launch and residence in space.

5. Characteristics of forced precession

In a state of forced precession, the **L** vector of a rotating body executes a cone about an axis in space that is determined by the nature of an applied torque. This axis forms the natural direction for the inertial –axis in the standard 3-1-3 Euler angle sequence, so that $\dot{\varphi}$ is along that axis. Note that this involves a different choice of coordinate systems that of free precession, because here the z-axis is defined as the axis about which **L** precesses, rather than the **L**-axis itself. In the standard analysis of a symmetric top undergoing forced precession, $\dot{\psi}$ is directed along the symmetry axis of the top (as in free precession), it represents the largest component of spin, and it is approximately equal to the rotation rate. **L** therefore points nearly along the symmetry axis (Fig.6a). However, for forced

Figure 8: Standard Euler angle development for forced precession of symmetric top (a) is not convenient for the typical case of a tumbling RB.

precession of a tumbling RB, the standard Euler angles are not particularly convenient, since precession is about a transverse axis so axial roll must be treated by varying θ.

The rate at which **L** precesses about the symmetry axis due to torque **τ** is given by

$$\frac{d\phi}{dt} = \frac{\tau}{L\sin\theta} \tag{24}$$

There are only two torques that are relevant for tumbling RBs in LEO: those due to magnetically induced eddy currents, and the gravity gradient torque. These are treated in the following sections.

6. Gravity gradient torque

The gravity gradient torque exists due to the slight change in the force of gravity across the length of satellite. For our case of a symmetric cylinder, the magnitude of this torque can be expressed as:

$$\tau_g = -\frac{GM_e \Delta I}{r^3}\sin(2\alpha_g) \tag{25}$$

where α_g is the angle between the long axis and the geocentric vector, defined here as the unit vector directed from the center of mass of the cylinder toward the earth's center. The direction of the torque is given by the cross product of the x_{3b} body axis and the geocentric vector. With point masses m_1 and m_2 placed at the ends (see Fig.8a), the above result is replaced by

$$\Delta I_{new} = \Delta I + M\tilde{z}^2 + m_1\left(\frac{H}{2} - \tilde{z}\right)^2 + m_2\left(\frac{H}{2} + \tilde{z}\right)^2 \tag{26}$$

where

$$\tilde{z} = \frac{H}{2}\left(\frac{m_1 - m_2}{M + m_1 + m_2}\right) \tag{27}$$

This modification allows investigation of the effects of adding masses to the cylinder.
For a satellite in circular orbit, it is easily shown that the equation of motion for the angle $2\alpha_g$ is that of a pendulum in the angle $2\alpha_g$:

$$I_0\ddot{\alpha}_g = -\frac{GM_e \Delta I}{r^3}\sin(2\alpha_g) \tag{28}$$

If the angular velocity is close to the orbit period, Eq. (27) gives simple harmonic motion about either $\alpha_g = 0$ or π with frequency:

$$\omega_g = \sqrt{\frac{2GM_e \Delta I}{I_0 r^3}} \tag{29}$$

For an SL-8 at an altitude of 600km, the period of these oscillations is

$$P_g = \frac{2\pi}{\omega_g} \approx 1.3 hr \tag{30}$$

The period of oscillations is an excellent, intuitively useful measure of the strength of the torque: gravity gradient torque only becomes important for SL-8s when rotation period slows to ~ 1.3 hours, when capture into the state of synchronous rotation is imminent. Note that this period is very close to the orbital period in LEO, suggesting that spin-orbit resonances may be possible for such satellites. Interestingly, the ratio of gravity gradient oscillation period to the orbital period depends only on the satellite inertia components:

$$\frac{P_{grav}}{P_{orbit}} = \left(\frac{I_0}{2\Delta I}\right)^{\frac{1}{2}} \approx 0.8 \text{ for SL-8s} \tag{31}$$

It may be that slowly rotating satellites in orbits with nonzero eccentricity exhibit large oscillations about either of the stability points ($\alpha_g = 0,\pi$) due to the resonant interactions with the time-varying gravitational force. Given the estimates of components for SL-8s used in this paper, it also appears that resonant commensurabilities exist near ratios of orbit period to rotation period of 4/5 and 7/8. The practical consequence of these interactions would be that when rotation periods are close to the orbit period, chaotic rotation or large librations about these points may occur. We should not be surprised to find that the symmetry axes of slowly rotating RBs are directed away from the geocentric direction.
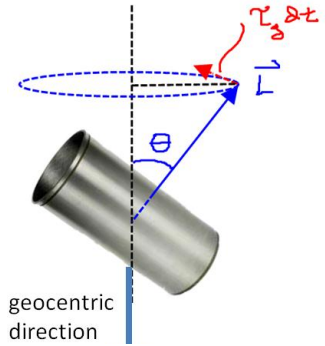

Fig.9: Precession geometry due to gravity gradient torque acting on tumbling RB.

Gravity gradient torque may also produce a slow precession of the rotation axis of a more rapidly rotating satellite (rotation period << orbit period) that is nearly in a state of flat spin. The situation is shown in Fig.7. Using the results described previously, the precession period is:

$$P_g = \frac{2\pi^2 I_0 r^3}{GM_e \Delta I P_{rot} \cos\theta} \tag{32}$$

For an SL-8 with a rotation period of 60 seconds at an altitude of 600km, the precession period is nearly two weeks. For typical RBs, it is clear that precession rates due to gravity gradient torque is unlikely to generate precession rates that are observable within observations made during a single orbital flyby.

7. Magnetic eddy current torque

Electrical eddy currents are induced in rotating, electrically conducting satellites through Faraday's Law, as the flux due to the geomagnetic field passing through the object continually changes. Through the Lorenz force, these currents result in a torque on the satellite that is a linear function of the angular velocity components. Components of the torque oppose the angular velocity while others are at right angles to the components of omega. Therefore this torque causes damping of omega and concommitant precession. Eddy current torque depends on the cube of the geocentric distance, so they are most significant in LEO. Numerous papers have been written on the topic of eddy current torques acting on cylindrical satellites, but all assume a specific rotation state, and furthermore the torques are typically averaged over the orbit period, which limits the results to cases where the angular velocity changes slowly relative to the orbit period. Smith [7] computed the torques for two specific cases: axial spin and pure tumble. Due to the linearity of the equations, careful examination of the differing coordinate systems and variables defined by Smith allows a single expression to be deduced, that is valid for all orientations of the angular velocity relative to the RB. In this manner, we find:

$$
\begin{bmatrix} \tau_1 \\ \tau_2 \\ \tau_3 \end{bmatrix} = A' \begin{bmatrix} B_1 B_2 \omega_3 - B_3^2 \omega_1 \\ B_2 B_3 \omega_3 - B_3^2 \omega_2 \\ \left(B_1^2 + B_2^2\right)\omega_3 + B_1 B_3 \omega_1 + B_2 B_3 \omega_2 \end{bmatrix} \tag{33}
$$

where

$$
A' = \pi \sigma R^3 l t \left[1 - \left(\frac{2R}{l}\right) \tanh\left(\frac{l}{2R}\right) \right] \tag{34}
$$

In this equation the B_i are the components of the magnetic field, measured in the body coordinate system. The constants in A' are:

σ = electrical conductivity of shell
t = thickness of cylinder walls
l ,R= length and radius of rocket body

The precession generated by the magnetic torque has a period given by

$$
P_{mag} = \frac{2\pi}{\frac{d\phi}{dt}} = \frac{2\pi L \sin\theta}{\tau_{mag}} = \frac{2\pi I_0 \sin\theta}{A' B^2} \tag{35}
$$

For the same SL-8 parameters described in the previous section, and given the earth's dipole moment is m~8x10^{22} Am^2, P_{mag} is on the order of a few months, and so it is comparable to the gravity gradient torque. Due to this torque, it is found in [7] that typical satellite spin components in the equatorial plane of the earth damp in ~9 days, and ~90 days for spin axis parallel to the earth's dipole axis.

It is of academic interest to note that τ_{mag} goes to zero only when the RB has zero angular velocity, yet the gravitational torque vanishes only for a finite (synchronous) rotation state. It can be shown that an RB in a simple polar orbit will consequently have a stable state in which α_g is slightly nonzero (~.01 degrees), while a negligibly small but finite amount of orbital energy is continuously transformed into heat via the eddy currents, causing the orbit to experience very slight decay.

8. A coordinate system framework for simulations of rotation states

In order to perform numerical integrations of the equations of motion and to relate the rotational dynamics of an RB to telescopic observations, a rotational evolution code was created in Matlab. The code includes the orbital elements, observation site coordinates, the Greenwich Mean Sidereal Time of the observations, and a set of coordinate systems that allow transformation of vectors between the body coordinate system, the coordinate system of the earth's dipole field and of the observation site, and other intermediate coordinate systems. Space does not allow a full description here, but by defining a few important coordinate systems, it will be possible for the reader to understand our preliminary results. The body coordinate system is defined such that the x3b-axis is directed along the symmetry axis of the RB, and the other two axes correspond to the two maximum principal axes (Fig.8a). The inertial "I" coordinate system, (x_I, y_I, z_I) is defined such that the x_I and y_I axes are in the equatorial plane, with the x_I-axis directed toward the satellite's ascending node (Fig.8b).
Also shown in Fig.8b is the gamma coordinate system, where the x and y axes are in the earth's equatorial plane, with the x-axis directed toward the vernal equinox. In order to include the magnetic eddy current torque in the equations of motion, the position vector of the RB is transformed to a coordinate system in which the earth's magnetic dipole field B is symmetric about the z-axis (not shown). The components of B are then computed at the satellite's location, and subsequently transformed to the body coordinate system, where they are input into the Euler equations. Numerical integrations are in progress. Figs.9a and 9b illustrate simulated light curves from an open-ended cylinder rotating in its minimum energy state (maximum axis rotation) , but here we show only the light curves corresponding to pure end-over-end motion (Fig.9a), and the same object with a 10-degree "wobble" as described in section 4 (Fig.9b).
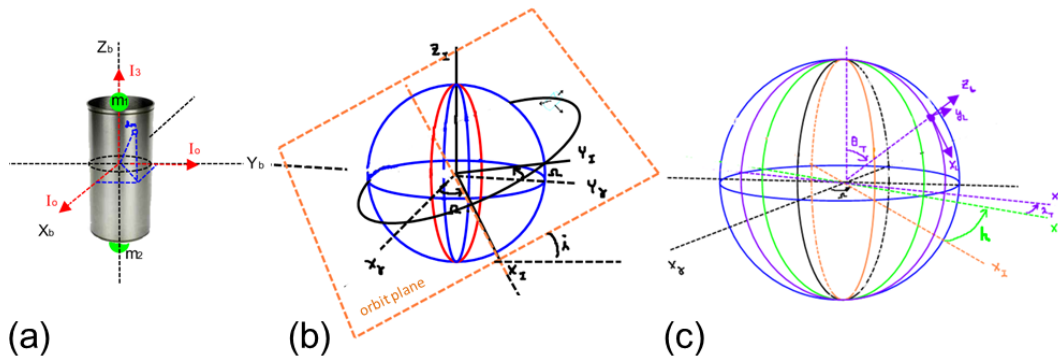
Fig. 9: Diffuse (red) and specular (yellow) intensities from a simulated RB seen from New Mexico Skies observatory. In case (a) no wobble (b) satellite has 10-degree wobble as defined in text.

The most immediately evident difference between cases with and without wobble is that specular flashes occur at differing times. This is understandable, since specular flashes only occur when the phase angle bisector is parallel to a surface normal vector, so that tipping of the long axis due to wobble will change the occurrence of this condition.
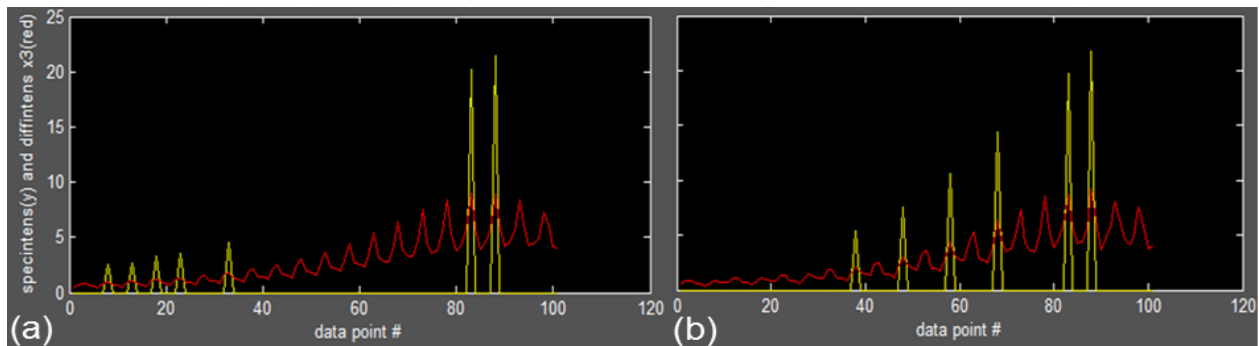

Fig. 9: Diffuse (red) and specular (yellow) intensities from a simulated RB seen from New Mexico Skies observatory. In case (a) no wobble (b) satellite has 10-degree wobble as defined in text.

If desired, the program simultaneously outputs a video of the RB as seen from the observation site. Figure 10 is an example of a video frame from the program's output. The yellow, green, and magenta lines represent the directions toward the sun, the observer, and the angular velocity vector, respectively. So that the green line is not reduced to a point, the view is rendered from a location a few degrees away from that of the observer's location.

9. Discussion and conclusions

The characteristics of realistic rotation states for cylindrical RBs undergoing free precession and forced precession have been examined in some detail. It is found that in free precession, values of the roll rate psidot are comparable to the rate of precession (phidot) of the long axis about

Fig. 10: Output frame from Matlab observation simulation program. See text.

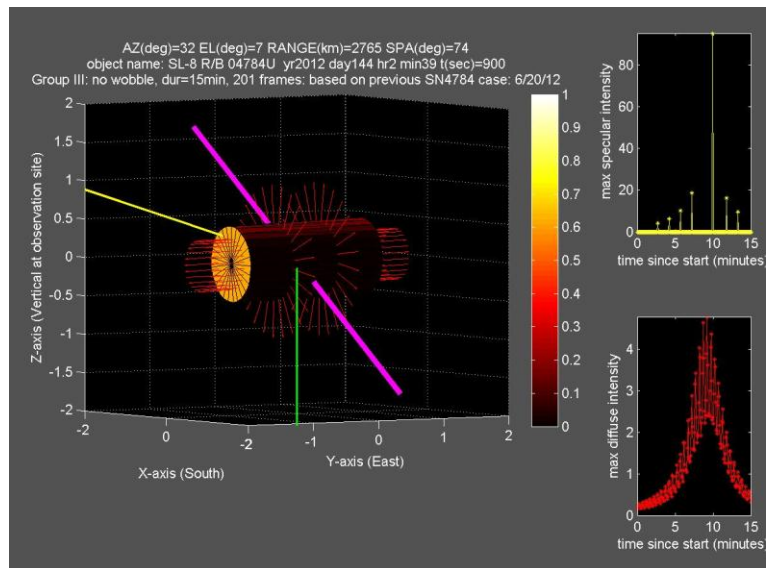the angular momentum direction in inertial space, until the object is within only a few percent of the minimum

energy rotation state. Furthermore, estimates of rates of internal dissipation as functions of the coning angle theta, or alternatively, of the energy, suggest that dissipation may slow dramatically as the minimum energy state is approached, so that theta may linger within several degrees of a flat spin for an extended period of time. Although phidot is the primary modulator of the light curve signal as flat spin is approached, it is not identical to the rotation rate because of the persistence of significant roll rate psidot. RBs with assymmetric mass distributions, for which the principal axes of inertia are offset from the symmetry axes, will be indistinguishable from RBs that are undergoing free precession, unless they have noticeably non-axisymmetric reflection characteristics. For Soviet SL-8s, the saddle tanks may produce roll-rate signatures of ~25% variation in light curve intensity, which may be observable and could provide confirmation of estimated values for phidot and theta, through the relationship given in equation (3). Alternatively, if detectable in telescopic observations, colored insignias, present typically on one side of RBs at launch, would generate signals providing an ideal measure of phidot. The only torques large enough to generate significant forced precession are the gravity gradient torque and the magnetically induced eddy current torque. However, for typical rotation rates near flat-spin conditions, these torques can only cause precession periods of weeks to months, whereas free precession rates are comparable to the rotation rate. Published claims of rotation periods, precession periods, and coning angles that do not conform to these specifications (e.g., Toshi's paper) are therefore necessarily erroneous. When slowing rotation rates approach the mean motion, large deviations of orientation from the commonly expected state where the long axis is directed toward the geocenter may be common, due to the proximity of spin-orbit commensurabilities. Numerical integrations of the full Euler equations of motion for an RB are under development. These integrations include the effects of the eddy currents, gravity gradient torque, and internal friction.

11. References

1. Liou, J.-C. (2011) An active debris removal parametric study for LEO environment remediation, Advances in Space Research 47 (2011) 1865–1876.

2. C. Wetterer; M. Jah, "Attitude Determination from Light Curves", Journal of Guidance, Control, and Dynamics, Vol.32, NO.5, 2009, pp. 1648-1651.doi: 10.2514/1.44254

3. Moriba, K.J., Ronald, A.M. Satellite characterization: angles and light curve data fusion for spacecraft state and parameter estimation, in:AMOS conference (http://www.amostech.com/), 2007

4. Yanagisawa, T. and H. Kurosaki (2012) Shape and motion estimate of LEO debris using light curves. Advances in Space Research 50, 136–145.

5. Rosenstock, Herbert B.: The Effect of the Earth's Magnetic Field on the Spin of the S a t e l l i t e . Astronautica Acta, Vol. 111, Fasc. 3, 1957,pp. 215-221.

6. Smith, G. L. (1962). A theoretical study of the torques induced by a magnetic field on rotating cylinders and spinning thin wall cones, cone frustums, and general bodies of revolution. NASA. TR-R-129.

7. Smith, G. L. (1964). Effects of magnetically induced eddy-current torques on spin motions of an earth satellite. NASA. TN-D-2198.

8. Williams,V, and Meadows, A.J.(1978).Eddy Current Torques, air torques, and the spin decay of cylindrical rocket bodies in orbit, J. Planetary and space science, V. 26, pp. 721-726.

9. Hughes, P.C. (1986). Spacecraft Attitude Dynamics. John Wiley & Sons, New York,

10. Marion, J.B, and S. T. Thornton (1995). Classical mechanics of particles and systems, 4th edition. Thomson Brooks/Cole Publishing, Pacific Grove, CA.

11. Vanyo, J.P. (1993). Rotating fluids in Engineering and Science. Dover Publications, Inc.

12. Somers, P. (2012) Cylindrical Satellite Spin Axis Characterisation, Proceedings of 2012 Canadian Astroconference, Quebec City, Canada.

13. Dr.P.Anz-Meador (2012), personal communication.